NOTE: this is a post-print version of the manuscript. Typos and errors may be present. The final version of the published work (that should be always cited) can be found here:

Filippo Berto, Pasquale Gallo, Paolo Lazzarin,

High temperature fatigue tests of un-notched and notched specimens made of 40CrMoV13.9 steel,

Materials & Design, Volume 63, 2014, Pages 609-619, ISSN 0261-3069,

https://doi.org/10.1016/j.matdes.2014.06.048.

(https://www.sciencedirect.com/science/article/pii/S026130691400497X)

Figures and tables at the bottom.

High temperature fatigue tests of un-notched and notched specimens made of 40CrMoV13.9 steel

Filippo Berto*, Pasquale Gallo, Paolo Lazzarin

University of Padua, Department of management and engineering, Stradella San Nicola 3, 36100, Vicenza, Italy

*Corresponding author, email: berto@gest.unipd.it, phone: +390444998754, fax:+390444998888

Abstract

The present paper summarizes data from uniaxial-tension *stress-controlled* fatigue tests on specimens made of 40CrMoV13.9 steel. Tests are performed varying temperature, from room temperature up to 650°C. This steel is commonly employed for hot-rolling of metals and it is subjected, in service, to a combination of mechanical and thermal loadings. Two geometries are considered: plain specimens and plates weakened by symmetric V-notches, with opening angle and tip radius being equal to 90 degrees and 1 mm, respectively. The present work is motivated by the fact that, at the best of authors' knowledge, only a limited number of works dealing with high-temperature fatigue are reported in the literature for the medium/high cycle fatigue regime; in particular, no results seem to be available for 40CrMoV13.9 steel when tested at elevated temperature in the presence of notch effects.

After a brief review of the recent literature, the experimental procedure is described in detail and the new data from un-notched and notched specimens are summarized in terms of stress range, at the considered temperatures, for a total of 60 new experimental data. Finally, fatigue data from un-notched and notched specimens are re-analysed by means of the mean value of the Strain Energy Density (SED).

Keywords: high temperature, high cycle fatigue, V-notch, fatigue strength, 40CrMoV13.9

Nomenclature

c_w	Parameter taking into account the nominal load ratio in the SED evaluation
E	Young's modulus
$F(2\alpha)$	Function used in the evaluation of the averaged SED for blunt notches

$H(2\alpha, R_c/\rho)$	Function used in the evaluation of the averaged SED for blunt notches
$Q(T)$	Averaging temperature depending function for blunt notches
k	Inverse slope of the fatigue curves
K_f	Fatigue strength reduction factor
$K_{t,n}$	Theoretical stress concentration factor (on the net area)
N	Number of cycles to failure
N_A	Reference number of cycles to failure
R	Nominal load ratio
R_c	Radius of the control volume under pure tension
T_σ	Stress-based scatter index (for 10-90% probabilities of survival)
T_W	Strain energy-based scatter index (for 10-90% probabilities of survival)
$\overline{W}$	Averaged value of the Strain Energy Density (SED) over the control volume (circular sector)

Symbols

2α	V-notch opening angle
ρ	Notch tip radius
σ_a	Nominal stress amplitude due to axial loading (referred to the net transverse sectional area specimens)
σ_A	Fatigue strength at N_A cycles to failure (both amplitudes referred to the net area)
ν	Poisson's ratio

Abbreviations

SED	Strain Energy Density

1. Introduction

Hot-rolling process is increasingly required for higher mechanical performances, fatigue strength and quality of laminated products. Different steels have been employed in a large variety of applications to combine static and fatigue properties with an excellent wear resistance at high

temperature and in corrosive environments. Dealing with un-notched specimens, the fatigue behavior of different materials at high temperature has been investigated by some researchers [1-3].

In [1] an experimental investigation was conducted on 22Cr-20Ni-18Co-Fe alloy at elevated temperature using plain specimens. Fatigue tests were carried out at a constant temperature (871°C) while the strain ranged from 0.265 to 1.5 %. The fatigue lives varied from 10^3 to 10^6 cycles to failure. Cyclic deformation properties of the tested material were obtained from the tests and three fatigue models were applied discussing the advantages and drawbacks of each model.

The fatigue properties and crack growth mechanism of a 2.25Cr–1Mo steel were investigated in Ref. [2]. The study was aimed to investigate the fatigue life up to 10^7 cycles of structural components used in hot and high-pressure environments. The tests were conducted on un-notched specimens in a temperature range varying between 20 and 500°C. The high-cycle fatigue life was found to be strongly influenced by the density and size of interior inclusions.

Dealing with 1.25Cr0.5Mo steel, high-temperature stress controlled tests were carried out at different loading conditions to investigate the fatigue–creep interaction behavior at high temperatures [3]. Four fatigue–creep facture maps were obtained showing that for stress amplitudes lower than the mean stress a close interaction between fatigue and creep occurred. This interaction provoked a visible reduction of the fatigue strength. The complex relationship between the fatigue life and the main influencing factors was explained by means of the strain rate at half-life, which was considered as the governing factor associated with the fatigue strength. Moreover, based on the ductility exhaustion theory and the effective stress concept, a new model for the fatigue–creep life assessment under stress control was proposed providing a master curve for fatigue–creep life prediction.

The increasing working temperature range and the growing necessity for greater efficiency and reliability of automotive exhaust system has been requiring the accurate investigation of the fatigue properties of heat resisting stainless steels at high temperature. In [4] ferritic stainless steels, such as 409L, 436L and 429EM STS were tested in a temperature range from 600 to 800 °C, which is

typical for exhaust system during the common operations of a vehicle. The fatigue strength of 429EM was found to be higher than those of the other two steels and significantly reduced by increasing temperatures. The thickness effect on the fatigue life was also investigated by varying the thickness of the specimen in a range from 1 to 2 mm. A complete insensitiveness was observed in the considered range.

Fully reversed axial fatigue tests were performed in [5] on smooth specimens of 18Cr–2Mo ferritic stainless steel (type 444) at room temperature, 673 K and 773 K in laboratory air, with the aim to investigate the effect of temperature on high cycle fatigue behavior. A notable influence of temperature on the fatigue strength was observed during the tests. At all temperatures, cracks nucleated at the specimen surface due to cyclic slip deformation, and crack initiation occurred earlier at elevated temperatures than at room temperature. Moreover, the crack growth was found to be considerably faster at elevated temperatures than at room temperature and some fractographic analyses revealed brittle features in fracture surfaces near the crack initiation site, which were more pronounced and extensive at 773 K. An evident embrittlement occurred in the investigated temperature range and such embrittlement was found to be the main responsible for the observed decrease in the fatigue properties.

In Ref. [6] the experimental investigation involved three different steels. A commercial martensitic P92 steel was tested at elevated temperature as well as two martensitic steels, reinforced with either 0.007% of boron (VY2 steel) or 0.2% of titanium (Ti1 steel) to improve their long term creep strength. All materials were austenitized at a temperature higher than 1150 °C for 30 minutes and tempered at 720 °C for 10 h. Creep–fatigue tests were carried out with tensile holding periods at 550°C. A physically-based model was proposed to assess the creep–fatigue lifetime of the considered steels. The model takes into account the crack density and the effect of the grain size on the crack initiation which are characteristic parameters for each steels. The model results to be very sensitive to these parameters.

In [7] the high temperature low cycle fatigue (LCF) behavior of ACI HB20-type, a cast ferritic stainless steel, was investigated. Isothermal strain controlled fatigue tests were carried out at 600 °C and 800 °C. The total strain amplitude applied to the samples varied from ±0.25% to ±0.65% with a strain rate of 10^{-3}/s. The fatigue lifetime curves at each temperature were derived accordingly to the Basquin's and the Coffin–Manson's equations.

Dealing with non-ferrous materials, the effect of surface treatment on the stress/life fatigue behavior of a titanium Ti–6Al–4V turbine fan blade alloy has been recently investigated in the regime of 10^2–10^6 cycles to failure under fully reversed *stress-controlled* isothermal push–pull loading, between 25 and 550°C at a frequency of 5 Hz [8]. The fatigue behavior has been examined in plain specimens in the deep-rolled and laser-shock peened surface conditions, and compared to results on samples in the untreated (machined and stress annealed) condition. Although the fatigue resistance of the Ti–6Al–4V alloy declined with increasing test temperature regardless of surface condition, deep-rolling and laser-shock peening surface treatments were found to extend the fatigue lives by factors of more than 30 and 5–10, respectively, in the high-cycle and low-cycle fatigue regimes at temperatures as high as than 550 °C.

While results from un-notched materials are not so rare in the past and recent literature as just discussed, only few systematic investigations have been performed on notched specimens under fatigue loading at high temperature at medium-high cycle fatigue [9-12].

In [9, 10], the notched fatigue strength of the nickel-base superalloy Inconel 718 was investigated under rotating bending loading at room temperature and 500°C in air. The linear notch mechanics was employed to assess the fatigue strength at elevated temperature being for that material the small-scale yielding conditions satisfied also at elevated temperature.

The effect of notch types and stress concentration factors on low cycle fatigue life and cracking of the DZ125 directionally solidified superalloy was experimentally investigated in [11]. Single-edge notched specimens with V and U type geometries were tested at 850 °C with a stress ratio R =0.1. The notch radius varied from 0.2 to 3.6 mm while the notch opening angle varied from 0° to 120°.

The results revealed that the fatigue strength decreased with the elastic stress concentration factor, K_t, increasing from 1.76 to 4.35. The main conclusion of the paper was that K_t can be considered as a key parameter controlling the notch fatigue at least when the absolute dimensions of the tested notched specimens are similar.

In a recent contribution the present authors have summarized the results from uniaxial tension *stress-controlled* fatigue tests performed at 650°C on Cu-Be specimens [12]. Two geometries have been considered: hourglass-shaped specimens and plates weakened by a central hole. All fatigue data from un-notched and notched specimens have been reanalyzed there in terms of the mean value of the strain energy density evaluated, for the notched specimens, over a finite size control volume surrounding the highly stressed zone at the hole edge. This has permitted to summarize all fatigue data in a quite narrow scatter band.

The present work deals with high temperature fatigue tests of 40CrMoV13.9. The tested material is characterized by four different heat treatments able to assure a high strength at room and elevated temperatures. The most important application is cold or hot rolling of magnesium and aluminium alloys. The steel under investigation combines very good static and fatigue properties with an excellent wear resistance, also at high temperature and in corrosive environments. A complete set of data from notch specimens under torsion and combined tension and torsion loadings at room temperature has been recently provided by the present authors [13].

Other similar Cr steels have been widely investigated at room temperature (see, among the others, Refs [14-17]). In particular, the effect on microstructure and fatigue threshold of pure tension fatigue at a stress level below the fatigue limit and high cycle regime were studied in [14, 15] considering a 12Cr steel and a 40Cr steel characterized by different heat treatments. The effects of nitriding and shot-peening treatments on the tensile fatigue behavior of 42CrMo4 steel have been recently investigated in [16, 17] considering notches of different acuity.

At the best of authors' knowledge, a complete set of data from un-notched and notched specimens at high temperature is not available in the literature for 40CrMoV13.9. With the aim to fill this lack,

the present paper experimentally investigates the behavior of this steel at different temperatures ranging from room temperature up to 650°C. The aim of this study is to present a set of new results from high-temperature fatigue tests on 40CrMoV13.9 un-notched and notched specimens in the medium- and high-cycle regime (10^5–10^6 cycles). The tests have been performed under uniaxial tension and *stress-controlled* conditions. A final synthesis of the present results together with previous data from multiaxial tests (at room temperature) on the same material [13] is carried out by means of the Strain Energy Density (SED) approach, as recently made for Cu-Be alloys tested at elevated temperature [12].

2. Material properties and specimens geometry

2.1 Material

The material investigated in the present study is 40CrMoV13.9 steel, usually employed for hot-rolling of metals where the material is usually subjected to a combination of mechanical and thermal loading conditions. Preliminary static tensile tests on a standard specimen were carried out to evaluate the elastic and strength properties of 40CrMoV13.9 steel at 650°C: Young's modulus E is equal to 135 GPa, σ_Y is equal to 520 MPa and σ_R to 610 MPa. The data-sheet reports the following mechanical properties at room temperature (25°C): elastic modulus E is equal to 206 GPa, tensile strength of about 1300 MPa and a yield strength of 1100 MPa with a percent elongation of 15%. The properties (at room temperature and 650°C) are also summarized in Table 1.

The chemical composition of the material and the heat treatment schedules are given in Table 2 and Table 3, respectively. The material was first quenched at 920°C and subsequently tempered twice at 580°C and 590°C. A final stress relieving treatment at 570°C was carried out. The final microstructure was characterized by a high strength bainitic-martensitic structure. The microstructure of the specimens is shown in Fig. 1 at different magnification values. It is evident that the microstructure is homogenous along all the directions, also through the specimen thickness, due to the austenitizing and annealing processes.

2.2 Fatigue testing equipment

The fatigue tests are conducted on a servo-hydraulic MTS 810 test system with a load cell capacity of 250 kN. The system is provided with a MTS Model 653 High Temperature Furnace, as shown in Figure 2. It is ideal for a wide variety of high-temperature tests, including tension, compression, bending and fatigue testing of different materials, metallic and not. It has a center-split design that enables easy access to both grippers and specimens. The furnace includes the MTS digital PID Temperature Control System and is configured for two heating zones which can be independently temperature-controlled through high precision thermocouples. The zone at constant temperature is 80 mm length. The heating elements are made of silicon carbide. An insulation plate situated between the upper and lower elements helps to ensure reliable zone separation and pre-cut insulation reduces heat loss. This furnace is particularly well-suited for applications that require a lower thermal gradient on a fatigue (or tensile) specimen. The nominal temperature for this furnace ranges from 100°C to 1400°C and the control point stability is about ± 1°C. Since the wedge grips are affected by the heat of the furnace, they are equipped with a cooling system that keeps the temperature low enough in order to not provoke any damage to the test-instruments.

2.3 Procedure for fatigue testing

The concerned *stress-controlled* fatigue tests were carried out at temperature values ranging from 20°C to 650°C: the specimen was heated to reach the desired temperature and after a short waiting period (20 minutes) necessary to assure a uniform temperature, the test was started. The temperature was maintained constant until specimen failures thank to the PID temperature control system. The uniaxial tensile fatigue tests were carried out over a range of cyclic stresses at the constant frequency of 5 Hz; the nominal load ratio R was kept constant and equal to 0.

Two specimen geometries were considered:

- Hourglass shaped (smooth) specimens with a theoretical stress concentration factor close to 1.0 (see Figure 3);
- Plates weakened by lateral symmetric V-notches, with a net cross section of 20 mm × 5 mm and a total length of 300 mm (Figure 4). The notches were characterized by a depth, *a*, equal to 5 mm, an opening angle, 2α, equal to 90° and a notch tip radius ρ=1 mm. This geometry results in a theoretical stress concentration factor $K_{t,n}$=3.84 (on the net transverse sectional area).

The specimens were designed to avoid an increase of temperature near the grippers and the length of 300 mm, which is higher than the length usually adopted at room temperature, was chosen for this reason. Figure 5 shows an image of the tested specimens.

As stated above the *stress-controlled* fatigue tests were carried out at different temperatures. More precisely, the hour-glass shaped specimens were tested at room temperature, 360°C and 650°C; the V-notched specimens were tested at room temperature, 360°C, 500°C and 650°C. Overall, eight fatigue curves were obtained by testing more than 60 specimens.

3. Results and discussion

3.1 Fatigue curves

The fatigue data were statistically re-analysed by using a log-normal distribution and are plotted in term of nominal stress ranges (referred to the net area) in Figures 6 and 7. More specifically, Figure 6 shows the fatigue data of the hourglass specimens, the Wöhler curve (mean curve, P_s = 50%), the Haibach scatter band referred to 10% and 90% probabilities of survival (for a confidence level equal to 95%) and the inverse slope k of the curves. Data from specimens tested at room temperature and at T=360°C are found to belong to the same scatterband, with a value of the scatter index quite low, T_σ=1.29. The scatter of the specimens tested at T=650°, instead, is higher being T_σ=2.00, which show also a strong decrease of the fatigue strength combined with a strong variation of the slope. A vertical line is drawn in correspondence of one million cycles where the mean values of the stress range are given to make the

comparison easier. At 10^6 cycles the stress range is equal to 675.14 MPa when T≤360°C, while it is equal to 95.23 MPa at 650°C.

Fatigue data of the specimens weakened by lateral V-notches are shown in Figure 7 at different temperatures. The run-out specimens (marked by tilted arrow) were excluded from the statistical analysis. It is evident that up to 500°C there are no differences with respect to the room temperature, whereas a substantial decrease of fatigue strength can be observed at 650°C. The scatter-band related to the specimens tested at T=650°C is compared with that summarising data obtained for T≤500°C. At one million cycle, the value of the stress referred to a probability of survival of 50% decreases from 213.12 to 74.32 MPa. The variation of the slope is also strong, it decreases from k=5.14 to k=2.91. Conversely, the values of the scatter index are comparable.

For the sake of completeness, the results are also summarized in details in Table 4.

The drastic decrease of the fatigue properties observed at 650°C is linked to the specific heat treatments made on the material. The maximum temperature in the tempering treatment was equal to 590°C and the last stress relieving treatment was carried out at 570°C. Experimental data clearly document that under long time exposure at temperatures higher than 570-590°C all beneficial effects due to the heat treatments are lost.

3.2 Notch sensitivity

By comparing the reduction of the fatigue strength exhibited at 10^6 cycles by the notched specimens tested at room temperature with respect to un-notched ones, one determines a fatigue strength reduction factor K_f equal to 3.17, which is a little lower than the theoretical stress concentration factor $K_{t,n}$=3.84 obtained by means of a FE analysis (Ansys code) and in good agreement with the value provided by Peterson's handbook. This means that a notch root radius ρ=1 mm involves the notch sensitivity index is less than 1.0. It is worth noticing that the fatigue strength reduction factor K_f at 650°C is equal to 1.48, which is remarkably lower than the value determined at room temperature. It is evident that the high temperature has strongly reduced the notch sensitivity of the steel.

3.3 Fracture surfaces by Scanning Electron Microscopy

The final geometrical configuration of some broken specimens was analysed together to their fracture surfaces. Figure 8 compares plain specimens tested at room and elevated temperature (650°C), with comparable fatigue lives. It is evident that the specimen tested at high temperature shows, as expected, a more ductile fracture if compared with the specimen tested at room temperature. It is also evident the visible necking on the net sectional area before the final failure. The fracture surfaces were also found to be different when analyzed by means of the Scanning Electron Microscope (SEM) at the same magnification value (see Figure 9). At high temperature some signs of transgranular fracture can be detected, as well as the formation of numerous micro-voids (Figure 9a). These micro-voids are big if compared to that of room temperature fracture surfaces (Figure 9b). At last, the fracture surface of plain specimens tested at high temperature is relatively clean, without any oxidation of the surface occurred during the tests. This remark is very important because the oxidation is a key phenomenon at elevated temperature; it can strongly influence both the crack initiation and its propagation, drastically reducing the fatigue strength of the material exposed to this event. The oxide film, in fact, is continually disrupted under repeated cyclic of strain/stress and the enhanced locally oxidized region acts as a notch to further concentrate local strains and stresses. However, if certain conditions are satisfied, e.g. high load frequency and short time exposure at high temperature, there would be insufficient time for chemical effects to act [18-20].

Creep of materials is classically associated with time-dependent plasticity under a constant stress at elevated temperatures, which for steels are typically greater than 0.5 T_m (melting temperature) [18-20]. In the service conditions, the steel analysed in the present paper is usually employed for hot rolling applications where the temperature ranges between 400 and 650°C, which is approximately equal to 0.25-0.4 T_m. At this temperature, large deformations of the rolls as well as plasticity phenomena have to be avoided or minimized to guarantee a safe behaviour of the roll (within the

linear-elastic or small scale yielding conditions) and a satisfactory quality of the final laminated under the required lamination pressure. Under these conditions creep and fatigue interaction, as well as oxidation and ratchetting play a marginal role for the considered material. In particular, the time-dependent ratchetting is usually associated with creep and low cycle fatigue, as recently documented by Tong et al. [20] by utilizing different constitutive models.

Dealing with the fracture surfaces of V-notches, no significant plastic deformation was noted at failure in the vicinity of the notch tip at room temperature and at elevated temperature. Figure 10 shows two specimens failed approximately at the same number of cycles. The fracture surfaces of the V-notched specimens were found very similar at different temperatures, almost flat in the crack initiation zone. This is most due to the presence of the V-notch, that leads to a brittle behavior of the material also at high temperatures.

This observation was also supported by the SEM micrographs of Figures 11 and 12. At room temperature and at T=650°C, the fracture surfaces were found to be analogous near the notch tip where the crack initiation took place. No evident sign of micro-voids formation can be seen, nor evident signs of oxidation. At 650°C, two clear distinguishable zones of the fracture surfaces can be identified (see Figure 12): the bottom zone corresponds to the crack initiation and early propagation zone, the upper one corresponds to the final static failure. In this second zone, far away from the notch tip, small micro-voids similar (but smaller in diameter) to those detected on plain specimens (tested at high temperature) were observed.

4. A synthesis in terms of linear elastic SED averaged over a control volume

4.1 Strain energy density as a design parameter

The averaged strain energy density criterion (SED) states that failure occurs when the mean value of the strain energy density averaged over a given control volume surrounding the sharp or blunt

notch tip is equal to a critical value W_c [21, 22]. Under plane stress or plane strain condition the volumes becomes an area as depicted in Figure 13, where the radius of the control volume R_c does not depend on the notch geometry. The SED-based method has been extensively used in the last years dealing with high cycle fatigue of welded joints and notched components [23-28]. It has been also employed to assess fracture data from cracked and notched specimens tested under static conditions [29-32].

A recent review of the method has been presented in [33], where the analytical frame and the main applications of the SED approach are documented in detail. Some links with Neuber's concept of "Elementary control volume", Sih's factor S and Gillemot's concept of "Specific absorbed energy" are underlined [33] with about four hundred citations to papers published over the last fifty years.

Under mode I fatigue loading, the radius R_c of the control volume can be estimated as a function of the high cycle fatigue strength of plain specimens, $\Delta\sigma_{1A}$, and the range of notch stress intensity factor, ΔK_{1A}, both values typically referred to 5×10^6 cycles [21]:

$$R_c = \left(\sqrt{2e_1} \times \frac{\Delta K_{1A}}{\Delta \sigma_{1A}} \right)^{\frac{1}{1-\lambda_1}} \tag{1}$$

Parameters e_1 and λ_1 depend on the V-notch angle, according to Williams' solution. Equation (1) is valid also in the crack case, where the V-notch opening angle is zero. Under fatigue limit conditions, by introducing the threshold value of the stress intensity factor range for long cracks under Mode I conditions, ΔK_{th}, and the plain specimen fatigue limit, $\Delta\sigma_0$, one obtains:

$$R_c = \frac{(1+\nu)(5-8\nu)}{4\pi} \left(\frac{\Delta K_{th}}{\Delta \sigma_0} \right)^2 \quad . \tag{2}$$

where ν is the Poisson's ratio.

When ν=0.3, Eq. (2) gives R_c=0.845a_0, where $a_0 = (1/\pi)(\Delta K_{th} / \Delta\sigma_0)^2$ is the El Haddad-Smith-Topper parameter [34]. With reference to virtual plane stress conditions, (out-of-plane stress σ_z=0 in thin plates), simple algebraic considerations give:

$$R_c = \frac{(5-3\nu)}{4\pi}\left(\frac{\Delta K_{th}}{\Delta\sigma_0}\right)^2 \quad , \tag{3}$$

resulting in $R_c=1.025a_0$ for $\nu=0.3$. Relationships (2) and (3) prove the link between the radius R_c employed in the SED approach and the El-Haddad-Smith-Topper parameter a_0 under Mode I loading. For additional considerations on the characteristic length parameters used in local notch fracture criteria one should consult Ref. [35].

Dealing with blunt notches under fatigue loading the following expression can be used to evaluate the strain energy density range [23]:

$$\Delta\overline{W} = c_w F(2\alpha)\times H(2\alpha,\frac{R_c}{\rho})\times\frac{K_{t,n}^2\Delta\sigma_n^2}{E} \tag{4}$$

Here $\Delta\sigma_n$ is the stress range, $K_{t,n}$ is the theoretical stress concentration factor (both referred to the net sectional area), E is the Young's modulus. $F(2\alpha)$ depends on the notch opening angle and is equal to 0.705 for $2\alpha=90°$. Finally H depends both on the notch angle and the critical radius-notch tip radius ratio.

In order to unify in a common diagram the fatigue results from both R=−1 and R=0, the weighing parameter c_w has to be applied, according to the simple rule reported in Ref [23]. This rule states, in particular, $c_w=1.0$ for R=0 and $c_w=0.5$ for R=−1. As a result of the reduction of the effective SED, the fatigue strength range for R=−1 should theoretically increase according to a factor $\sqrt{2}$ with respect to the R=0 case.

4.2 Recent synthesis of multiaxial fatigue data from notched 40CrMoV13.9 steel by means of SED

The absence of data from 40CrMoV13.9 steel under multiaxial fatigue loading motivated a recent work by the present authors. Circumferential V-notched and semicircular notched specimens were tested under tension, torsion and combined tension and torsion, both in-phase and out-of-phase. The

results of the experimental programme consisted of 10 fatigue curves for a corresponding to more than 120 fatigue data [13].

The behaviour at medium and high cycle fatigue has been found to be within the elastic regime without any particular non-linear elastic effect. The approach based on the strain energy density averaged on a control volume has been employed to summarise all the data in a single scatterband. A single value of the control volume, R_c=0.05 mm, evaluated accordingly to the threshold stress intensity range reported in [14, 15] for Cr steels characterized by similar heat treatments, has been used in the synthesis, independently of the loading mode.

Figure 14 shows the final synthesis based on the averaged SED. Since all data come from specimens tested under the same nominal load ratio, R=-1, the coefficient c_w was not involved in [13].

The scatter index T_W, related to the two curves with probabilities of survival P_S= 10% and 90%, has been found equal to 1.96. The inverse slope of the scatterband is equal to 5.00. T_W=1.96 gives T_σ=1.40 when reconverted to an equivalent local stress range with probabilities of survival P_s=10% and 90%.

At the light of the results shown in Figure 14 it is clear that a single value of the control volume, independent of the loading modes, is sufficient to characterize the multiaxial fatigue behavior of 40CrMoV13.9 steel at room temperature. The synthesis in terms of SED has confirmed the choice of the control volume, being the obtained scatterband narrow enough in comparison with those obtained in previous works [21-28]. It is evident that the SED is able to summarize all the data in a single scatterband independently of the loading mode and notch geometry.

4.3 High-temperature fatigue strength of a copper-cobalt-beryllium alloy by means of SED

In order to extend to the high temperature fatigue the criterion based on the strain energy density over a control volume, a recent study has been performed on a copper-cobalt-beryllium alloy [12].

Beryllium copper alloys are commonly classified in two general categories: high strength and high conductivity alloys. The Cu-Be alloy investigated in [12] belonged to high conductivity class usually used for production of shells for hot rolling.

Since high temperature data from the cracked Cu-Be alloy were not available (e.g. ΔK_{th}), the critical radius R_c= 0.6 mm has been estimated by equating the values of the critical SED at $2x10^6$ cycles as determined from the plain and the notched specimens.

At $2x10^6$ cycles, by using the mean value of the stress range from plain specimens (241 MPa), the SED range was found to be 0.22 MJ/m^3.

The idea of using, under mode I loading, the linear elastic SED also in case of small scale yielding conditions was motivated in Refs [36-38]. A reformulation of Glinka's ESED approach applied no longer at the notch tip [36] but to a finite size circular sector surrounding the notch tip has been proposed in [37]. Under plane strain conditions, the value of the energy concentration due to the notch is constant and independent of the constitutive law. When small scale yielding conditions are satisfied this immediately results in the constancy of the strain energy averaged over the control volume. These important considerations are in well agreement with results by other researchers investigating the fatigue behaviour of Inconel 718 at room temperature up to 500°C [9, 10]. Chen et al., in fact, arrived to the final conclusion that Linear Notch Mechanics is applicable not only at room temperature but also at elevated temperature, as long as the small-scale yielding condition is satisfied.

The high temperature fatigue data of Cu-Be alloy, recently obtained by the present authors, are plotted in terms of averaged strain energy density range in Figure 15 [12], considering the aforementioned critical radius. Thanks to the SED approach it has been possible to summarize in a single scatterband all the fatigue data, independently of the specimen geometry, estimating also the characteristic radius for the considered material at high temperature.

5. Synthesis based on SED of the new high temperature data from 40CrMoV13.9

The new high temperature data from unnotched and notched specimens made of 40CrMoV13.9 are summarized in this section by using the SED approach. On the basis of the experimental evidences of the present work, the synthesis in terms of SED has been carried out up to 500°C considering the same critical radius used in Ref. [13] for multiaxial fatigue data, briefly recalling here in Section 4.2. In fact, as visible from Figures 6 and 7, no reduction in the fatigue strength has been detected until 500°C both for unnotched and notched specimens.

In the medium and high cycle fatigue regime the critical SED range for un-notched specimens can be simply evaluated by using the following expression:

$$\Delta\overline{W} = \frac{c_w}{2E}\Delta\sigma_n^2 \tag{5}$$

In Eq. (5) $\Delta\sigma_n$ is the nominal stress range referred to the net sectional area. As already said, the weighting parameter c_W has to be applied to take into account different values of the nominal load ratio. Being the actual tests referred to R=0, c_w is equal to 1.0. Since Eq. (5) is applied at different temperatures, the Young's modulus has to be updated as a function of the temperature.

E is equal to 206 GPa at room temperature and 135 GPa at 650°C. In the intermediate cases a linear trend has been assumed according with Ref. [39]. For a temperature of 360°C the Young's modulus E results to be 165GPa and at 500°C it is equal to 150 GPa.

For the notched specimens Eq. (4) can be directly applied. For the specific case of $2\alpha=90°$ and $R_c/\rho=0.05$, parameters F and H are equal to 0.7049 and 0.5627, respectively [23]. The stress concentration factor referred to the net area is equal to 3.84.

By using Equations (4, 5) the new data from the tests carried out at room temperature up to 500°C can be summarized in Figure 16 in a single narrow scatterband, characterized by an inverse slope k equal to 5.31 and a scatter index T_W equal to 2.25. Involving now the room temperature data from multiaxial tests on the same material [13] (Figure 14), it is possible to obtain a single scatterband, as shown in

Figure 17. It must be underlined that the multiaxial tests has been carried out at R=-1, and for this reason the weighting parameter c_w=0.5 introduced previously in the Section 4.1, has to be employed in order to convert the data in terms of effective SED range. Thanks to the SED approach it has been possible to summarise in a single scatterband all the fatigue data, independently of the specimen geometry, of the loading condition, and of the temperature, up to 500°C.

Dealing with data carried out at 650°C, the fatigue strength of unnotched and notched specimens has been found strongly lower than the corresponding data from tests carried out at T<500°C. For this specific temperature (T=650°), which is important in practical industrial applications, in particular for hot rolling of aluminum alloys, an empirical formula has been proposed for notched specimens by modifying Eq. (4). This allows us to take into account the notch sensitivity of this material at temperatures higher than 500°C:

$$\Delta\overline{W} = c_w Q(T) L(f/f_0) F(2\alpha) \times H(2\alpha, \frac{R_c}{\rho}) \times \frac{K_{t,n}^2 \Delta\sigma_n^2}{E} \quad (6)$$

Q (T) is the notch sensitivity function at a specific temperature T. This function has to be set (as a function of the temperature T) by equating at high cycle fatigue (10^6 cycles) the SED value from plain specimens and those from notched specimens; f is the test frequency of notched specimens at high temperature and f_0 the test frequency of unnotched specimens at the same temperature. L is a function related to the sensitivity of the material to the load frequency and depends on the ratio f/f_0. Function L is required to be equal to 1.0 if $f=f_0$, a condition respected in all tests of the present analysis. The critical radius R_c is kept constant and equal to that obtained at room temperature (R_c=0.05 mm). Dealing with our specific case Q (T=650°C)= 0.18. Equation (6) can be re-written by substituting the numerical value of each function:

$$\Delta\overline{W} = 1.0 \times 0.18 \times 1.0 \times 0.7049 \times 0.5627 \frac{K_{t,n}^2 \Delta\sigma_n^2}{E} = 0.07139 \frac{K_{t,n}^2 \Delta\sigma_n^2}{E} \quad (7)$$

Where, as said above, $K_{t,n}$=3.84.

By considering Eq. (7) applied to notched specimens and Eq. (5) applied to plain specimens, the SED master curve for 40CrMoV13.9 at 650°C has been obtained. The fatigue data from tests at 650°C are plotted in terms of averaged strain energy density range over a control volume in Figure 18, considering the critical radius previously derived at room temperature. It is possible to observe that the scatter band is quite narrow, with the scatter index being T_W = 2.56 that results in T_σ=1.60 in terms of equivalent local stress range. The inverse slope of the scatterband is equal to 1.43. Thanks to the SED approach it is possible to summarise in a single scatterband all the fatigue data at the same temperature, independently of the specimen geometry.

Future developments will be devoted to set the proposed empirical equation to other geometries and temperatures. The idea is to further increase the temperature, in order to study the interactions between fatigue and creep. Another open point is the behavior of the same steel under different loading conditions, for example in prevalent mode II or in combined mode I and mode III loading conditions. Another important aspect worth investigating is the constraint effect through the plate thickness. It can play a fundamental role in fracture and fatigue assessment, as documented in [40, 41].

6. Conclusions

Fatigue tests and metallographic analyses were carried out on 40CrMoV13.9 steel for high temperature applications in order to investigate the fatigue strength of this material at high temperature, more precisely from room temperature up to 650°C. The work has been motivated by the fact that, at the best of authors' knowledge, only a limited number of works dealing with high-temperature fatigue are available in the literature and no results seem to be available from notched components made of this steel tested at elevated temperatures.

Two specimen geometries were considered: hourglass shaped and plate with double symmetric V-notches. Furthermore, a statistical analysis of fatigue data was carried out for both geometries. The data

obtained were first summarized in the fatigue curves and later re-analyzed in terms of the local energy density.

The main results are summarised as follows:

1. The tested alloy exhibits a good high temperature fatigue behaviour up to 500°. Until that temperature no reduction in the fatigue strength with respect to the room temperature has been detected.
2. Above 500°C, a significant reduction in fatigue strength is shown both for plain and V-notched specimens.
3. At 650°C the notch sensitivity of the present steel seems to be quite low. The inverse slope *k* is also very similar. It is equal to 2.48 for hourglass shaped specimens and 2.91 for plates weakened by lateral notches.
4. The high temperature mitigates the stress concentration effect: the experimental value of K_f has been found to be equal to 1.48, which is very low if compared with the theoretical stress concentration factor ($K_{t,n}$=3.84).
5. The strong reduction of the fatigue properties of the present material at 650°C can be attributed to the specific thermal treatments performed on it. In fact the material was first quenched at 920°C and subsequently tempered at about 580°C twice. A final stress relieving treatment at 570°C was carried out. The tempered temperature and final stress relieving temperatures were lower than 650°C. It seems that for a long time exposure at temperatures higher than 570-590°C the beneficial effects due to these specific treatments were lost.
6. All new data from tests carried at room temperature up to 500°C are summarized in terms of mean SED over a control volume with R_c=0.05 mm. A sound agreement in terms of SED has been found between the present results and those recently obtained from a large bulk of multiaxial tests performed at room temperature on the same material.

7. A quite narrow scatter band characterized by a limited value of the scatter index has been obtained by summarizing together new data and old multiaxial data [13] up to 500°C.

8. A specific master curve based on SED has been proposed for the considered steel tested at T=650°C. The scatter band makes possible to summarize together data from plain and notched specimens. Dealing with notched specimens an empirical expression has been also proposed for the SED calculation. The equation can be directly employed for practical applications of 40CrMoV13.9 steel at 650°C.

References

1. Krukemyer TH, Fatemi A, Swindeman RW. Fatigue Behaviour of a 22Cr-20Ni-18Co-Fe alloy at elevated temperature. J Eng Mater-T Asme 1994; 116:54-61.

2. Kobayashi H, Todoroki A, Oomura T, Sano T, Takehana T. Ultra-high-cycle fatigue properties and fracture mechanism of modified 2.25Cr–1Mo steel at elevated temperatures. Int J Fatigue 2006; 28:1633-1639.

3. Fan Z, Chen X, Chen L, Jiang J. Fatigue–creep behavior of 1.25Cr0.5Mo steel at high temperature and its life prediction. Int J Fatigue 2007; 29:1174-1183.

4. Ha TK, Jeong HT, Sung HJ. High temperature bending fatigue behavior of stainless steels for automotive exhaust. J Mater Process Tech 2007; 187:555-558.

5. Uematsu Y, Akita M, Nakajima M, Tokaji K. Effect of temperature on high cycle fatigue behaviour in 18Cr–2Mo ferritic stainless steel. Int J Fatigue 2008; 30:642-648.

6. Fournier B, Salvi M, Dalle F, De Carlan Y, Caës C, Sauzay M, Pineau A. Lifetime prediction of 9–12%Cr martensitic steels subjected to creep–fatigue at high temperature. Int J Fatigue 2010; 32:971-978.

7. Ko SJ, Kim YJ. High temperature fatigue behaviors of a cast ferritic stainless steel. Mat Sci Eng A-Struct 2012; 534:7-12.

8. Altenberger I, Nalla RK, Sano Y, Wagner L, Ritchie RO. On the effect of deep-rolling and laser-peening on the stress-controlled low- and high-cycle fatigue behavior of Ti–6Al–4V at elevated temperatures up to 550 °C. Int J Fatigue 2012; 44:292-302.

9. Chen Q, Kawagoishi N, Nisitani H. Evaluation of notched fatigue strength at elevated temperature by linear notch mechanics. Int J Fatigue 1999; 21:925-931.

10. Kawagoishi N., Chen Q. and Nisitani H. Fatigue strength of Inconel 718 at elevated temperatures. Fatigue Fract Engng Mater Struct 2000, 23; 209–216.

11. Shi DQ, Hu XA, Wang JK, Yu HC, Yang XG, Huang J. Effect of notch on fatigue behaviour of a directionally solidified superalloy at high temperature. Fatigue Fract Eng M 2013; 36:1288-1297.

12. Berto F, Lazzarin P, Gallo P. High-temperature fatigue strength of a copper-cobalt-beryllium alloy. J Strain Anal Eng 2013; DOI: 10.1177/0309324713511804.

13. Berto F, Lazzarin P, Marangon C. Fatigue strength of notched specimens made of 40CrMoV13.9 under multiaxial loading. Mater Design 2014; 54:57-66.

14. Nian L, Bai-Ping D, Hui-Jiu Z. On the relationship between fatigue limit, threshold and microstructure of a low-carbon Cr-Ni steel. Int J Fatigue 1984; 6:89-94.

15. Nian L, Bai-ping D. The effect of low-stress high cycle fatigue on the microstructure and fatigue threshold of a 40 Cr steel. Int J Fatigue 1995; 17:43-48.

16. Terres MA, Laalai N, Sidhom H. Effect of nitriding and shot-peening on the fatigue behavior of 42CrMo4 steel: Experimental analysis and predictive approach. Mater Design 2012; 35:741-748.

17. Terres MA, Sidhom H. Fatigue life evaluation of 42CrMo4 nitrided steel by local approach: equivalent strain-life-time. Mater Design 2012; 33:444-450.

18. Kassner M. Fundamentals of creep in metals and alloys. 2nd ed. Amsterdam: Elsevier; 2008.

19. Coffin LF. Fatigue at high temperature-Prediction and interpretation. P I Mech Eng 1974; 188:109-127.

20. Manson SS, Halford GR. Fatigue and durability of metals at high temperatures. Ohio: ASM International; 2009.

21. Tong J, Zhao LG, Lin B. Ratchetting strain as a driving force for fatigue crack growth. Int J Fatigue 2013; 46:49-57.

22. Lazzarin P, Zambardi R. A finite-volume-energy based approach to predict the static and fatigue behaviour of components with sharp V-shaped notches. Int J Fracture 2001;112: 275-298.

23. Lazzarin P, Berto F. Some expressions for the Strain Energy in a finite volume surrounding the root of blunt V-notches. Int J Fracture 2005; 135:161-185.

24. Lazzarin P, Sonsino CM, Zambardi R. A notch stress intensity approach to assess the multiaxial fatigue strength of welded tube-to-flange joints subjected to combined loadings. Fatigue Fract Eng M 2004; 27:127-140.

25. Radaj D, Berto F, Lazzarin P. Local fatigue strength parameters for welded joints based on strain energy density with inclusion of small-size notches. Eng Fract Mech 2009; 76:1109-1130.

26. Radaj D, Lazzarin P, Berto F. Fatigue assessment of welded joints under slit-parallel loading based on strain energy density or notch rounding. Int J Fatigue 2009; 31:1490-1504.

27. Berto F, Croccolo D, Cuppini R. Fatigue strength of a fork-pin equivalent coupling in terms of the local strain energy density. Mater Design 2008; 29:1780-1792.

28. Berto F, Lazzarin P. Fatigue strength of structural components under multi-axial loading in terms of local energy density averaged on a control volume. Int J Fatigue 2011; 33:1055-1065.

29. Lazzarin P, Berto F, Elices M, Gómez J. Brittle failures from U- and V-notches in mode I and mixed, I+II, mode. A synthesis based on the strain energy density averaged on finite size volumes. Fatigue Fract Eng M 2009; 32: 671-684.

30. Berto F, Lazzarin P, Marangon C. Brittle fracture of U-notched graphite plates under mixed mode loading. Mater Design 2012; 41:421-432.

31. Berto F, Campagnolo A, Elices M, Lazzarin P. A synthesis of polymethylmethacrylate data from U-notched specimens and V-notches with end holes by means of local energy. Mater Design 2013; 49: 826-833.

32. Berto F, Lazzarin P. A review of the volume-based strain energy density approach applied to V-notches and welded structures. Theor Appl Fract Mec 2009; 52:183-94.

33. Berto F. Lazzarin P. Recent developments in brittle and quasi-brittle failure assessment of engineering materials by means of local approaches. Mat Sci Eng R 2014; 75:1-48.

34. El Haddad MH, Topper TH, Smith KN. Prediction of Non-Propagating Cracks. Eng Fract Mech 1979; 11:573-584.

35. Pluvinage G., Capelle J. On characteristic lengths used in notch fracture mechanics Int J Fract 2014; 187: 187-197.

36. Glinka G. Energy density approach to calculation of inelastic strain-stress near notches and cracks. Eng Fract Mech 1985; 22:485–508.

37. Lazzarin P, Zambardi R. The Equivalent Strain Energy Density approach reformulated and applied to sharp V-shaped notches under localised and generalised plasticity. Fatigue Fract Eng M 2002; 25:917–928.

38. Lazzarin P, Berto F. Control volumes and strain energy density under small and large scale yielding due to tensile and torsion loading. Fatigue Fract Eng M 2008; 31:95-107.

39. Latella BA, Humpries SR. Young's modulus of a 2.25Cr-1Mo steel at elevated temperature. Scripta Mater 2004; 51:635-639.

40. Meliani MH,, Matvienko YG, Pluvinage G. Two-parameter fracture criterion ($K_{\rho,c}$-$T_{ef,c}$) based on notch fracture mechanics. Int J Fract 2011; 167:173–182.

41. Matvienko YG, Shlyannikov VN, Boychenko NV. In-plane and out-of-plane constraint parameters along a three-dimensional crack-front stress field under creep loading. Fatigue Fract Eng M 2013; 36: 14-24.

Tables

Table 1. Mechanical properties of 40CrMoV13.9

Temperature	Young's Modulus E (GPa)	Ultimate tensile strength σ_R(MPa)	Yield stress σ_Y(MPa)	Elongation to fracture A (%)	HRC
Room Temp.	206	1355	1127	15.2	52
650°C	135	610	520	23.5	35

Table 2. Chemical composition wt.%, balance Fe.

C	Mn	Si	S	P	Cr	Ni	Mo	V	Al	W
0.38	0.5	0.27	0.006	0.003	3.05	0.24	1.04	0.24	0.013	0.005

Table 3. Heat treatment schedules

	Heat treatment	Heating ratio (°C/h)	Temperature (°C)	Holding (hours)	Cooling
1	Quenching	100	920 ± 10	3	water
2	Tempering 1	100	580 ± 10	5	air
3	Tempering 2	100	590 ± 10	5	air
4	Stress relieving	100	570 ± 10	3	air

Table 4. Results from fatigue tests at different temperatures. Stresses referred to the net area. HG stands for hour-glass shaped specimens while V stands for V-notched ones.

Specimen – T (°C)	k	T_σ	σ_{max} ($1 \cdot 10^6$ cicli)		
			10% MPa	50% MPa	90% MPa
HG - amb. to 360°C	7.28	1.29	766.27	675.14	595.54
HG - 650°C	2.48	2.00	134.76	95.23	67.29
V - amb. to 500°C	5.14	1.48	259.66	213.12	174.92
V - 650°C	2.91	1.63	94.83	74.32	58.25

Figures

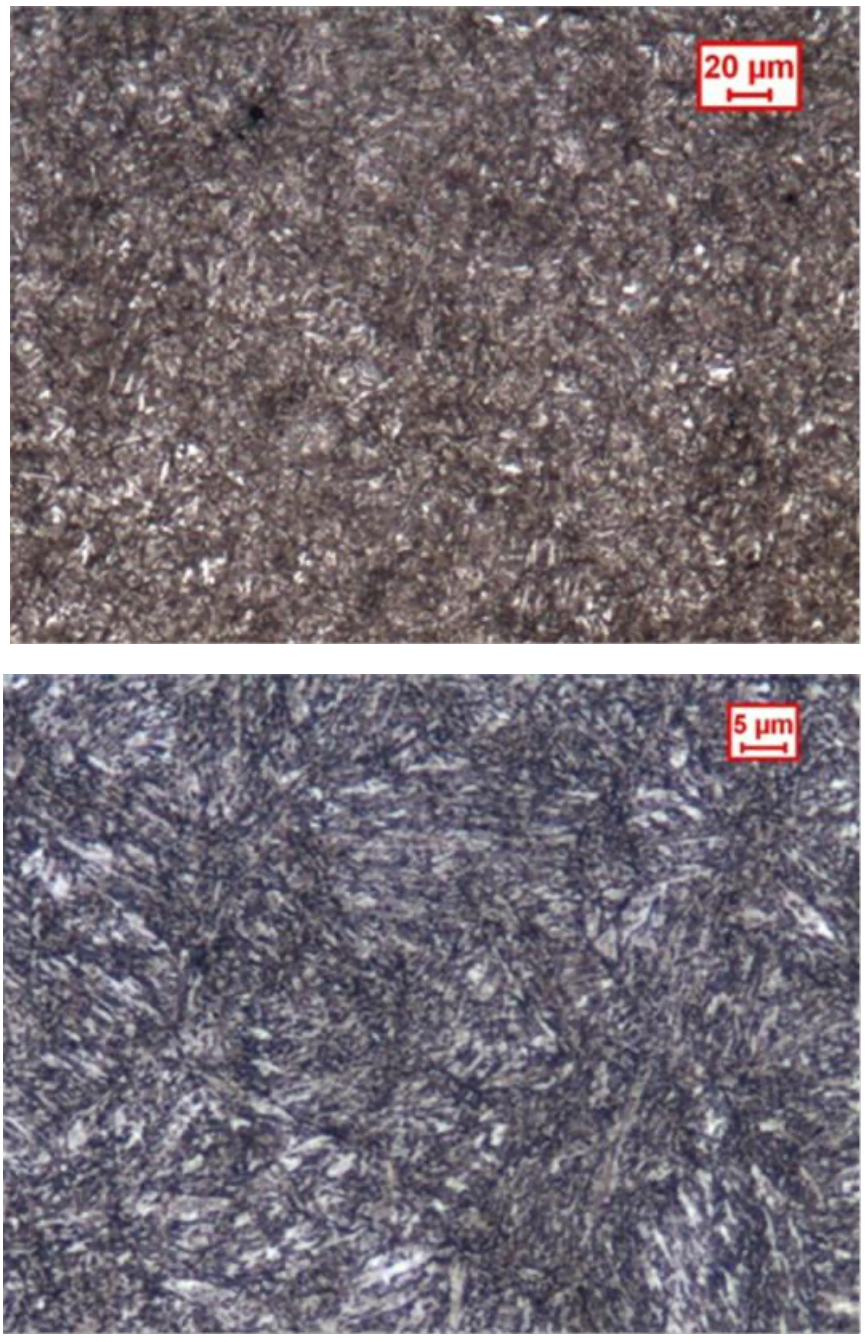

Figure 1. Microstructure of the specimens at different magnification values

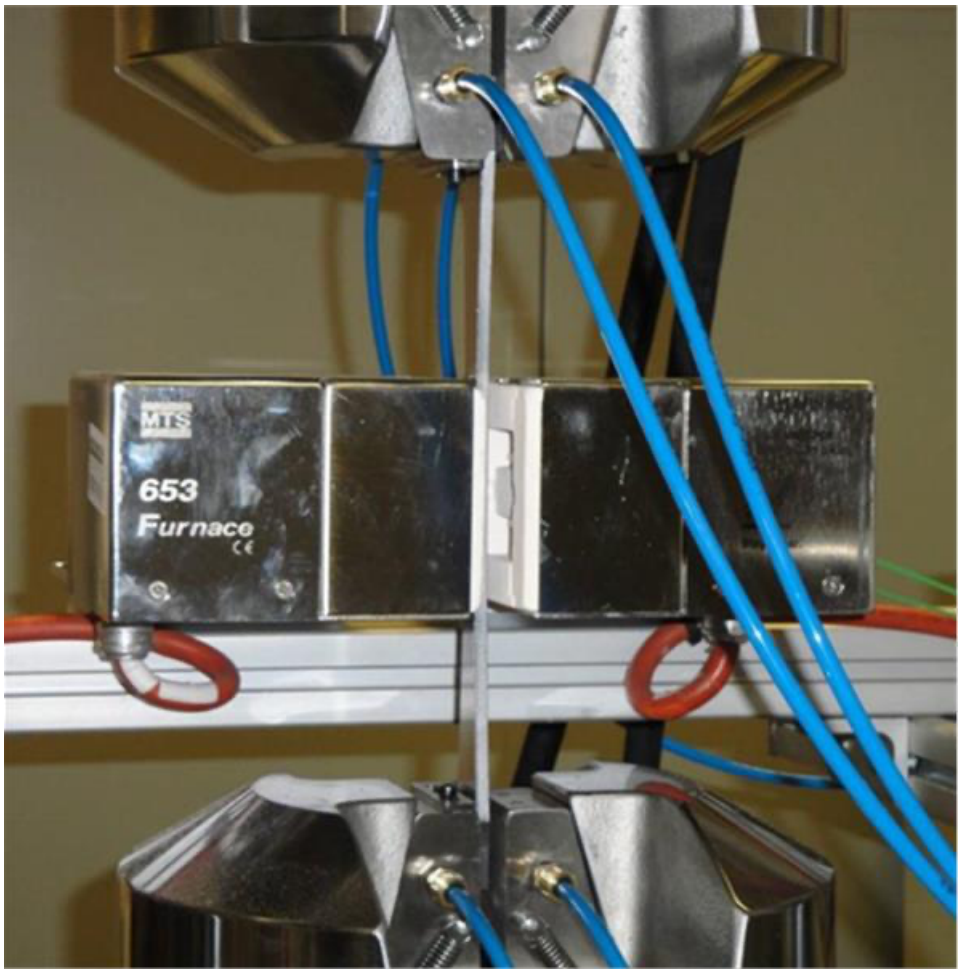

Figure 2. Fatigue test equipment for high temperature tests

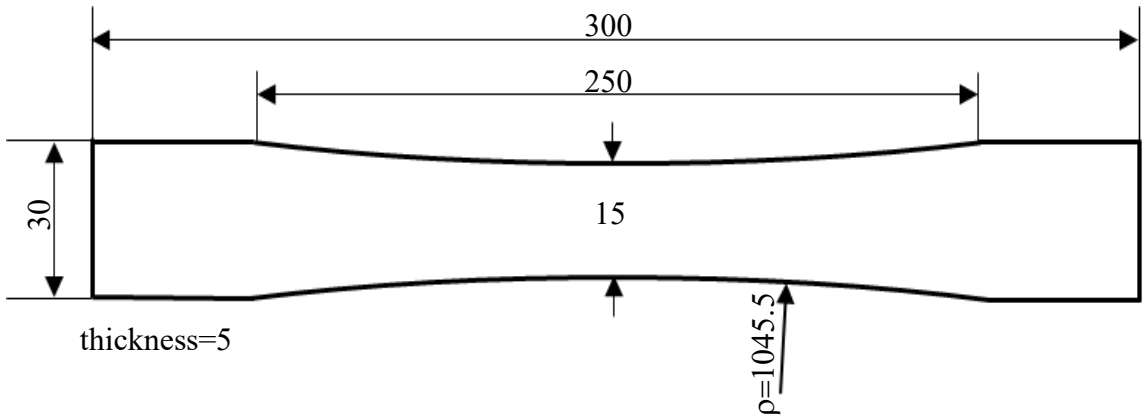

Figure 3. Hour-glass shaped specimen geometry, dimensions in mm

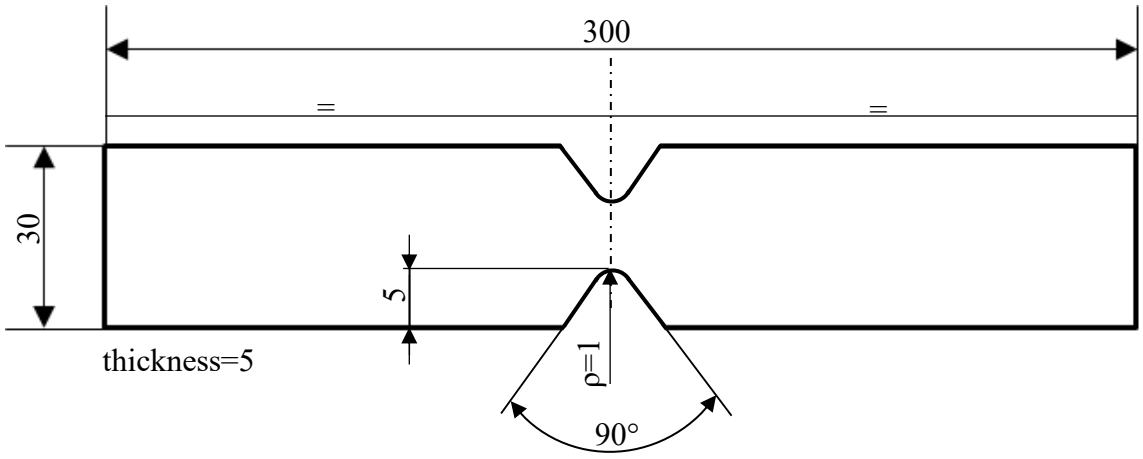

Figure 4. Notched specimen geometry, dimensions in mm

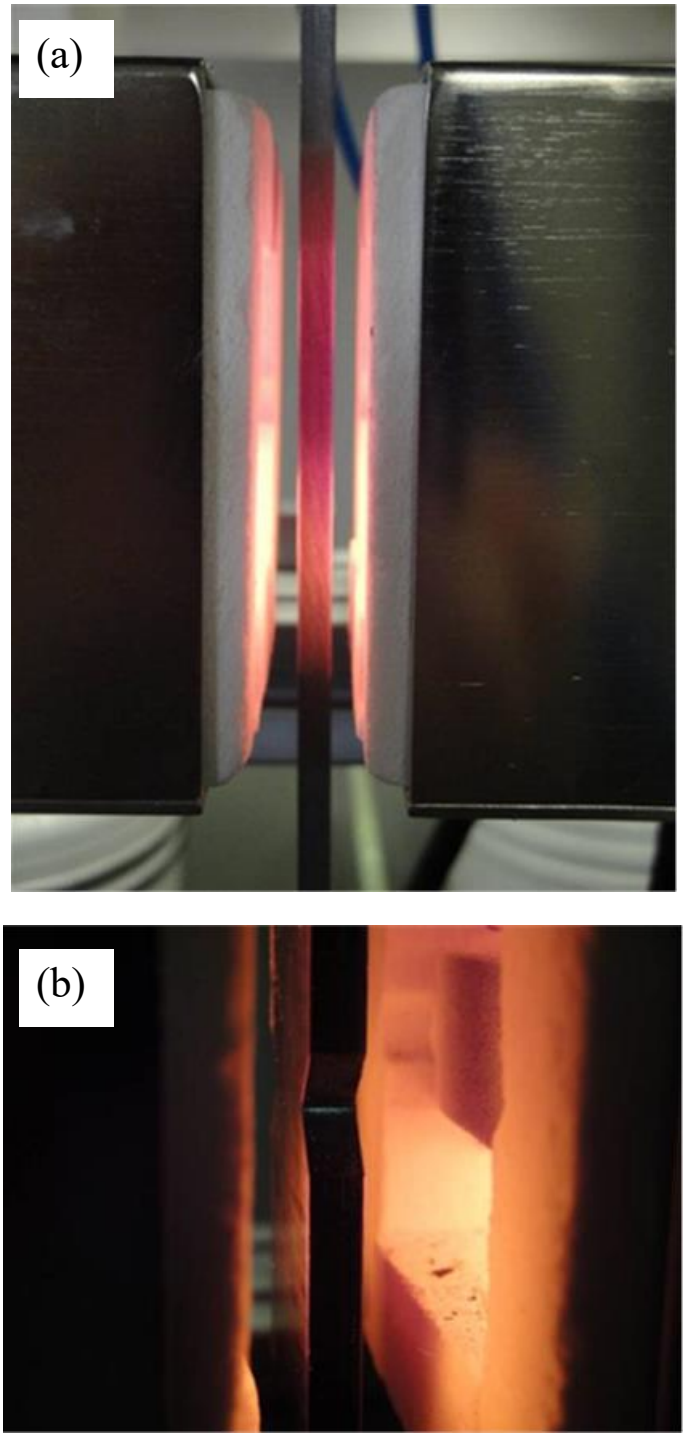

Figure 5. High temperature tests on plain (a) and notched specimens (b)

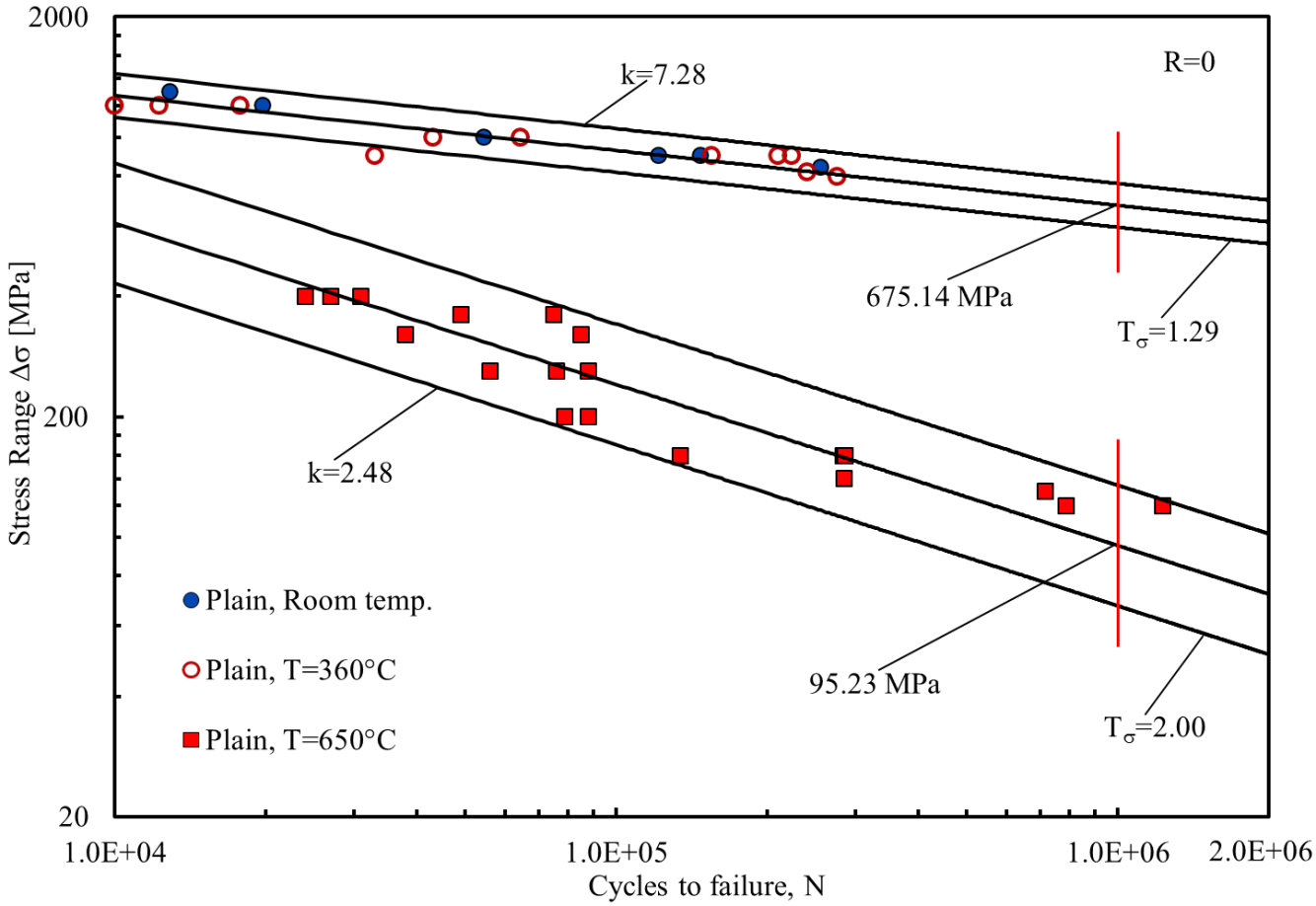

Figure 6. Data from hourglass shaped specimens at different temperatures

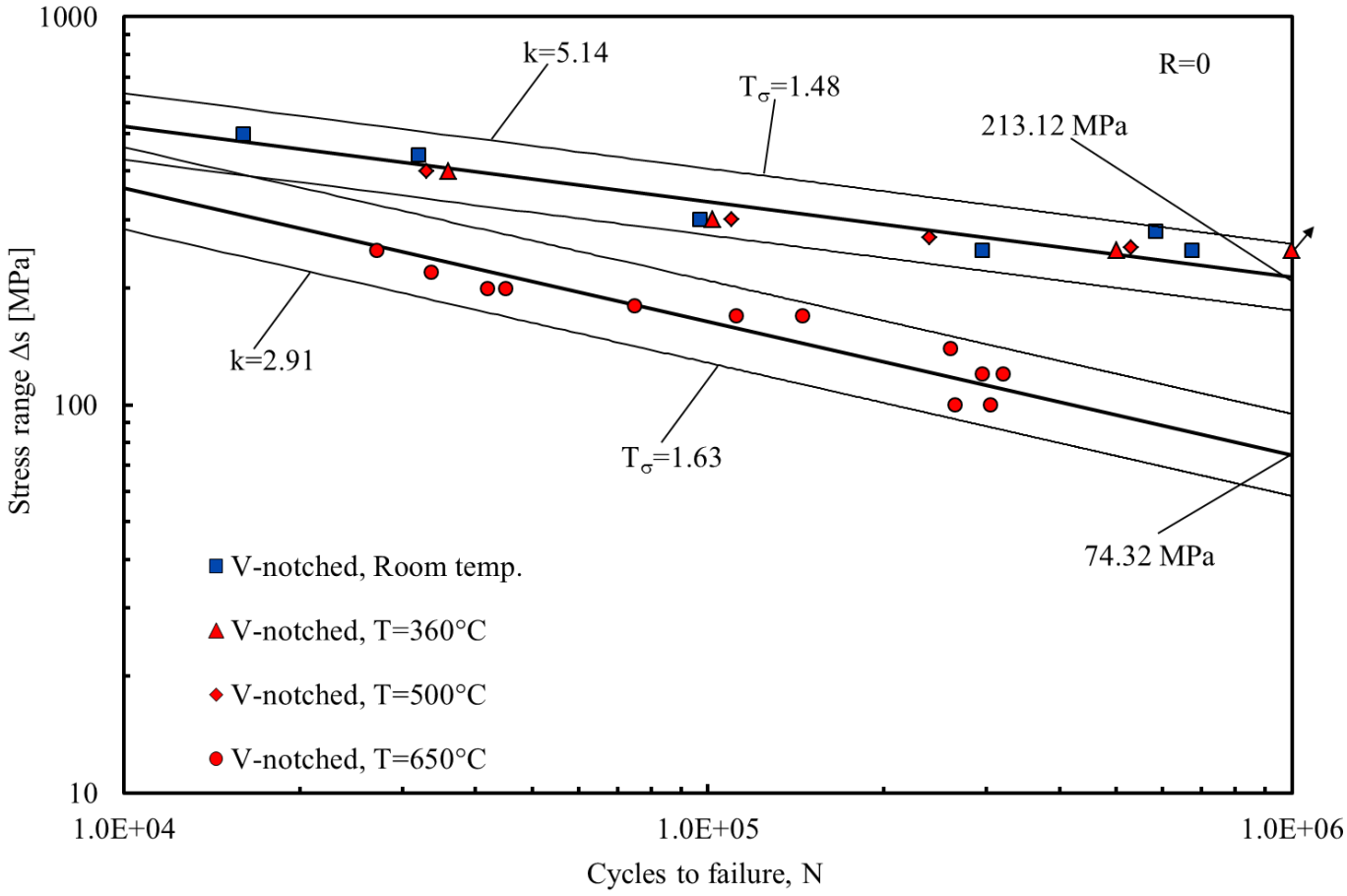

Figure 7. Data from V-notched specimens at different temperatures

Figure 8. Fracture surface of plain specimen tested at 650°C (a) (Δσ=140 MPa, N=284049), and room temperature (b) (Δσ=900, N=155000)

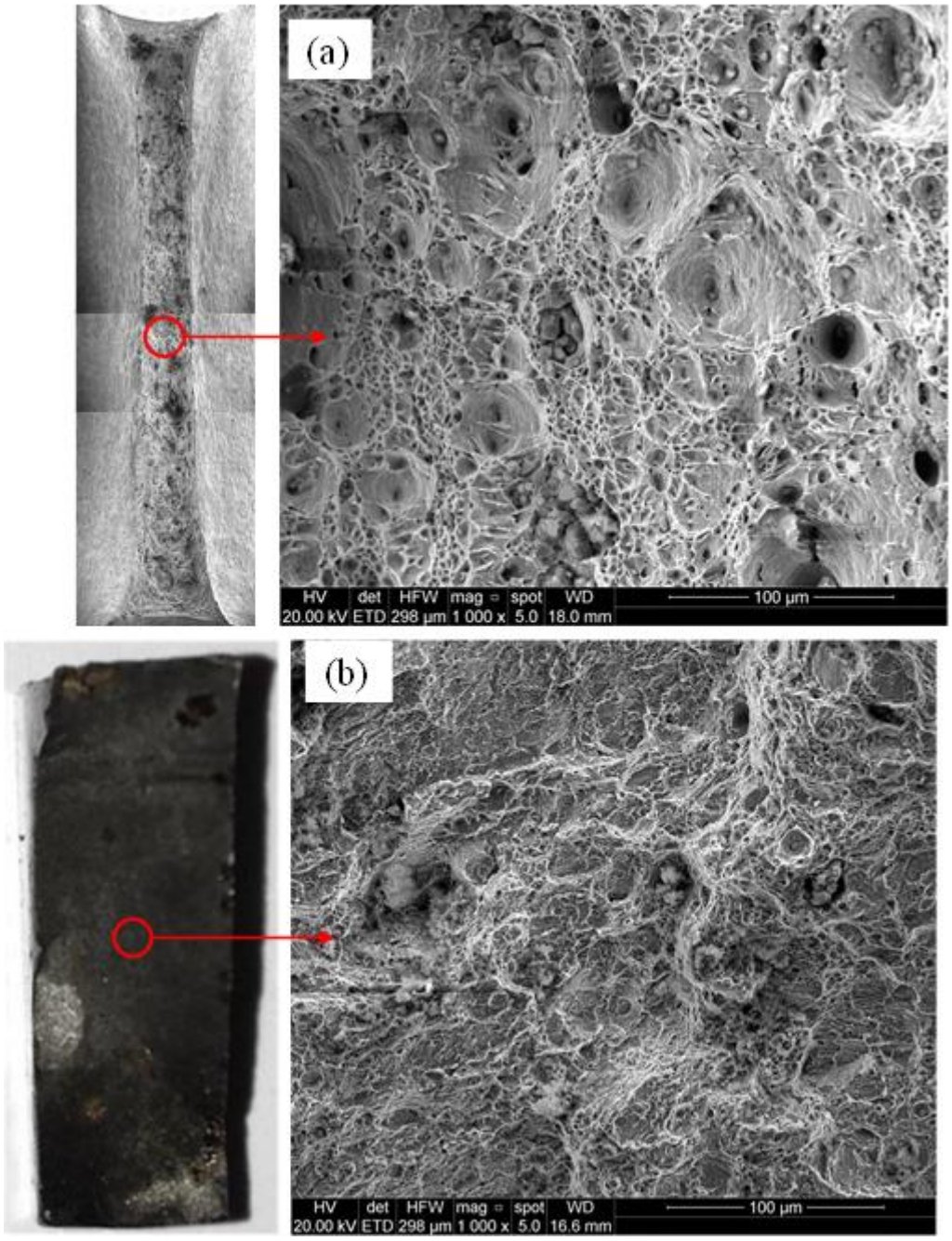

Figure 9 Comparison between the fracture surface of plain specimen tested at 650°C (a) ($\Delta\sigma$=140 MPa, N=284049) and room temperature (b) ($\Delta\sigma$=900, N=155000), considering the same magnification value

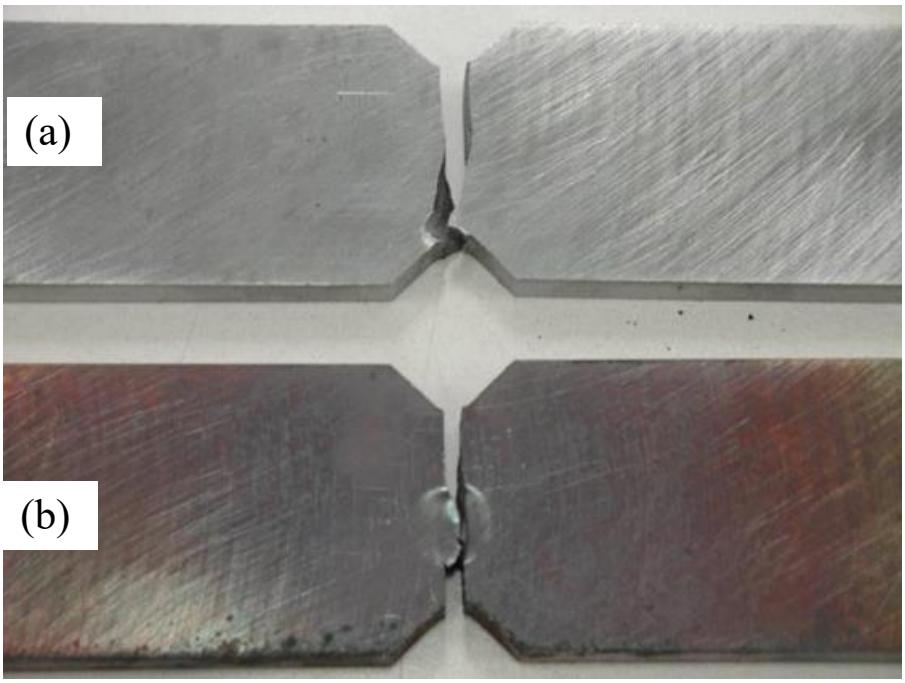

Figure 10 Fracture surfaces of the V-notched specimens tested at room temperature (a) (Δσ=250 MPa, N=295000) and high temperature (b) (Δσ=100 MPa, N=304000)

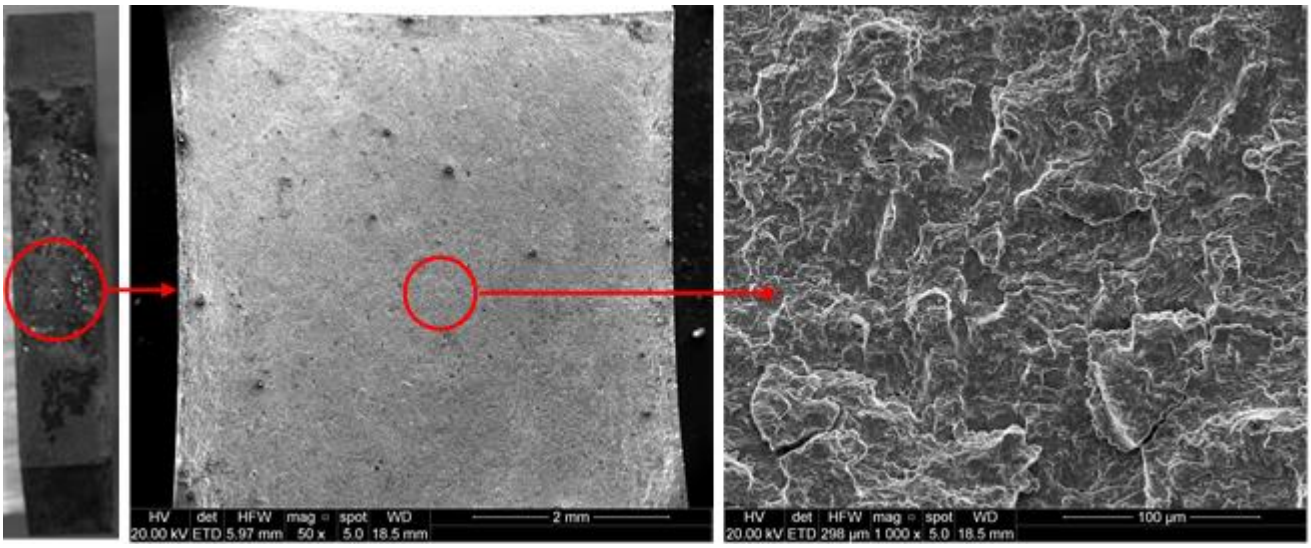

Figure 11. Details of the fracture surface of a notched specimen tested at room temperature (Δσ=250 MPa, N=295000)

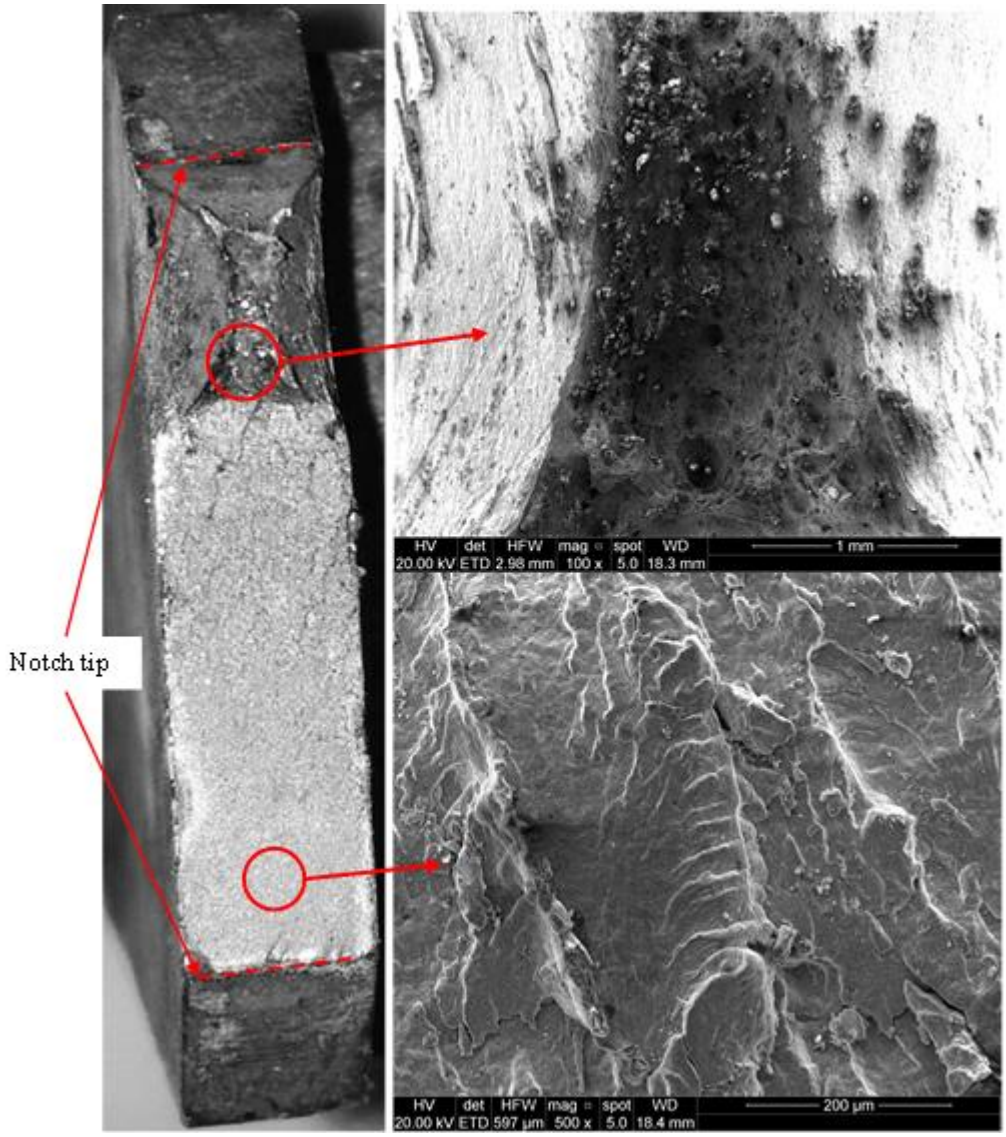

Figure 12. Fracture surface of a notched specimen tested at 650°C at different magnification values ($\Delta\sigma$=100 MPa, N=304000)

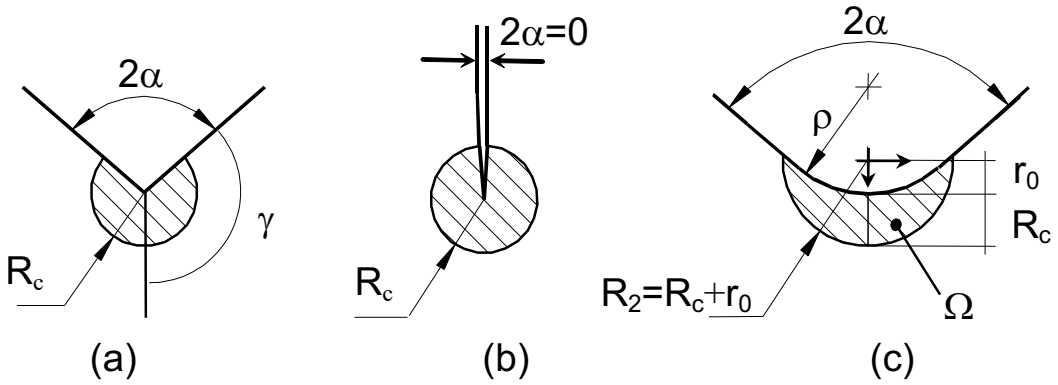

Figure 13. Critical volume (area) for sharp V-notch (a), crack (b) and blunt V-notch (c) under mode I loading. Distance $r_0 = \rho \times (\pi - 2\alpha)/(2\pi - 2\alpha)$

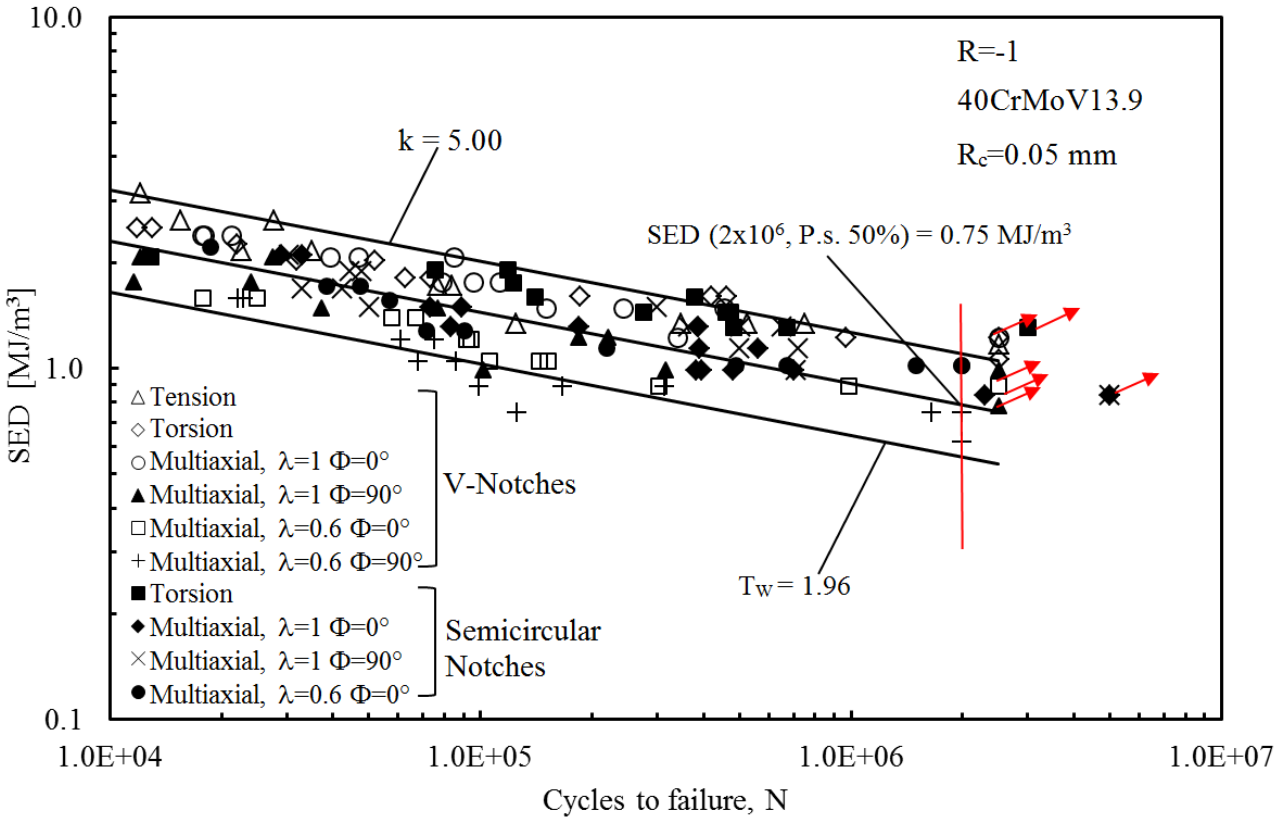

Figure 14. Synthesis by means of local SED of multiaxial series data at room temperature [13]

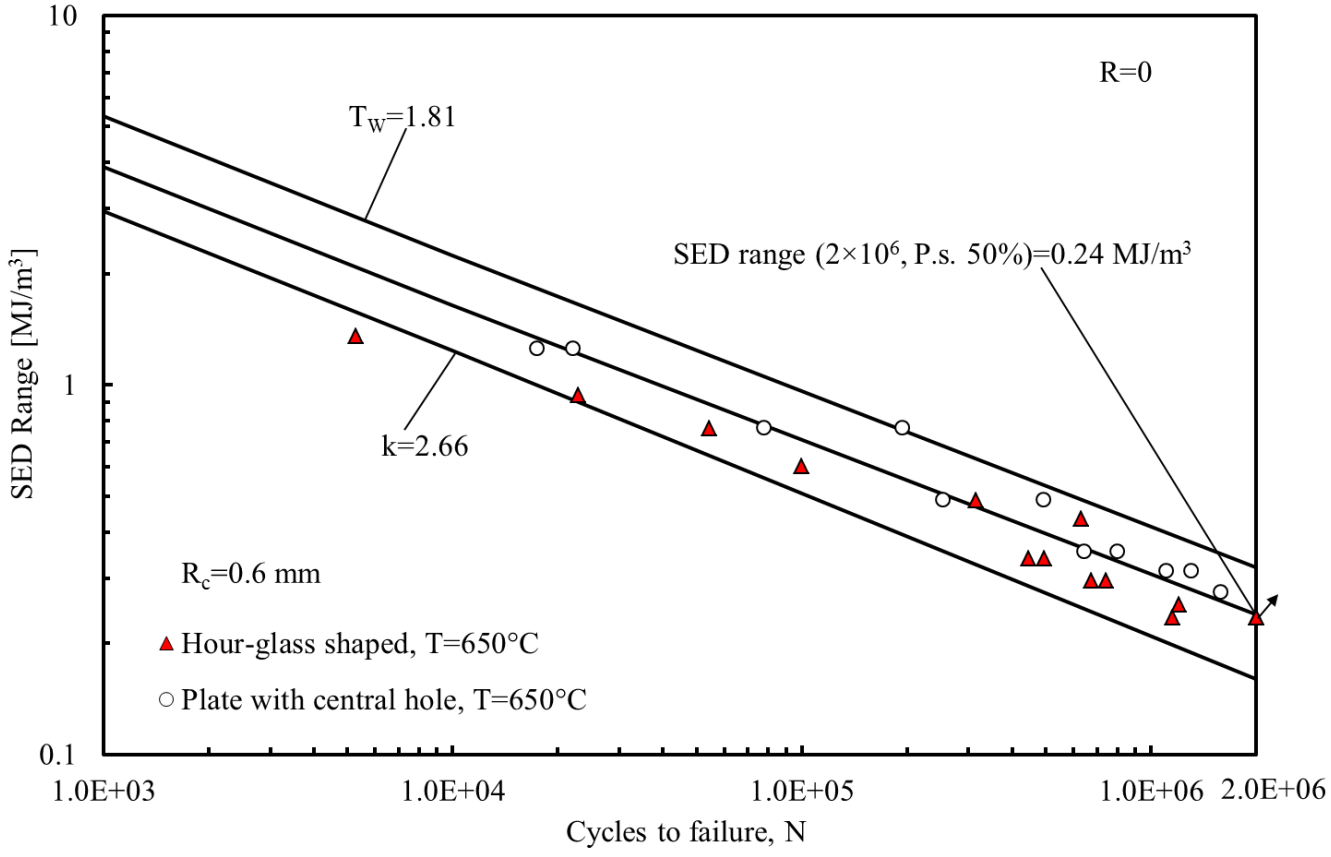

Figure 15. Synthesis by means of local SED of fatigue data from Cu-Be specimens [12]

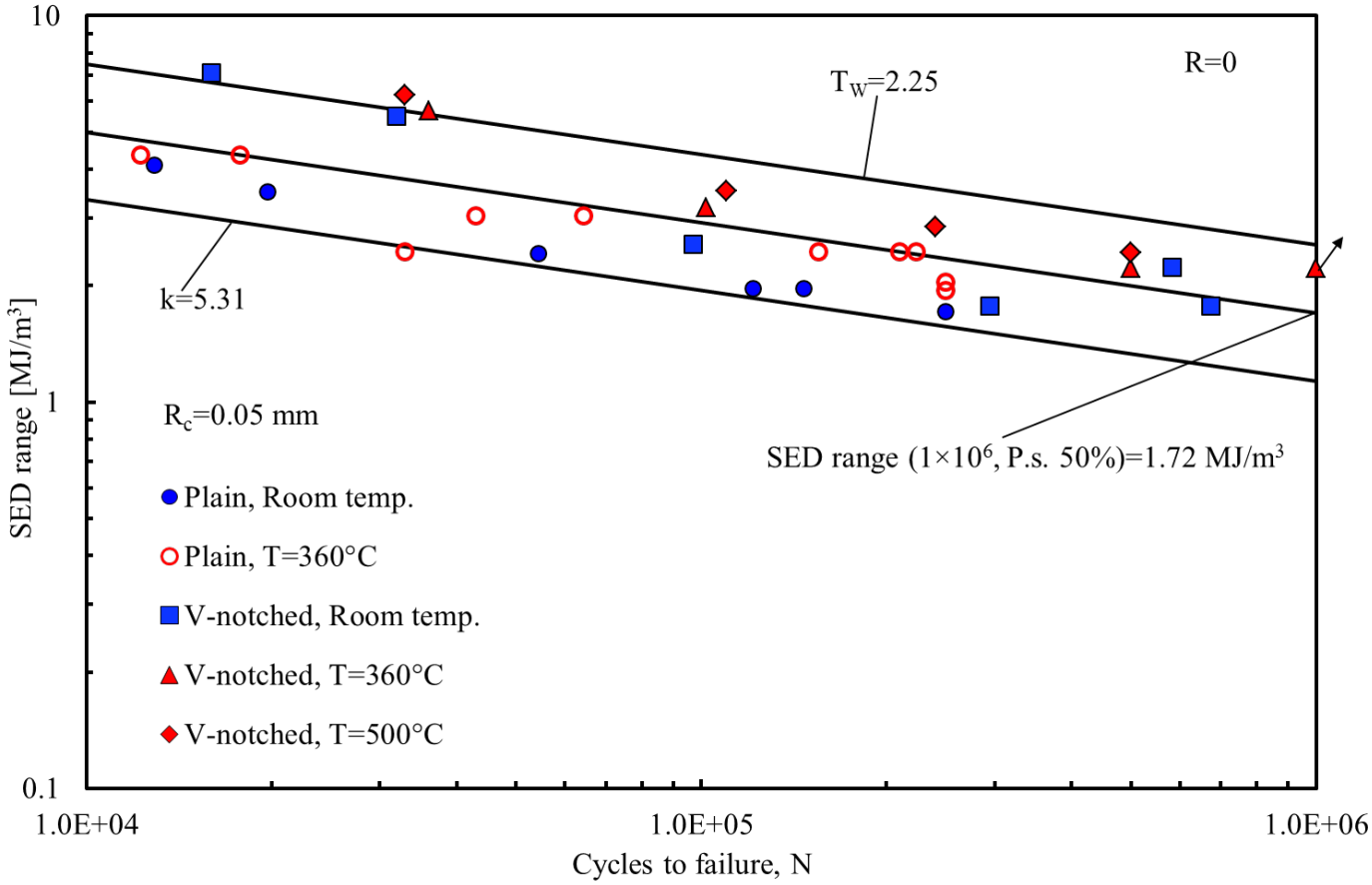

Figure16 Synthesis by means of local SED of new fatigue data from plain and V-notched specimens between room temperature and 500°C

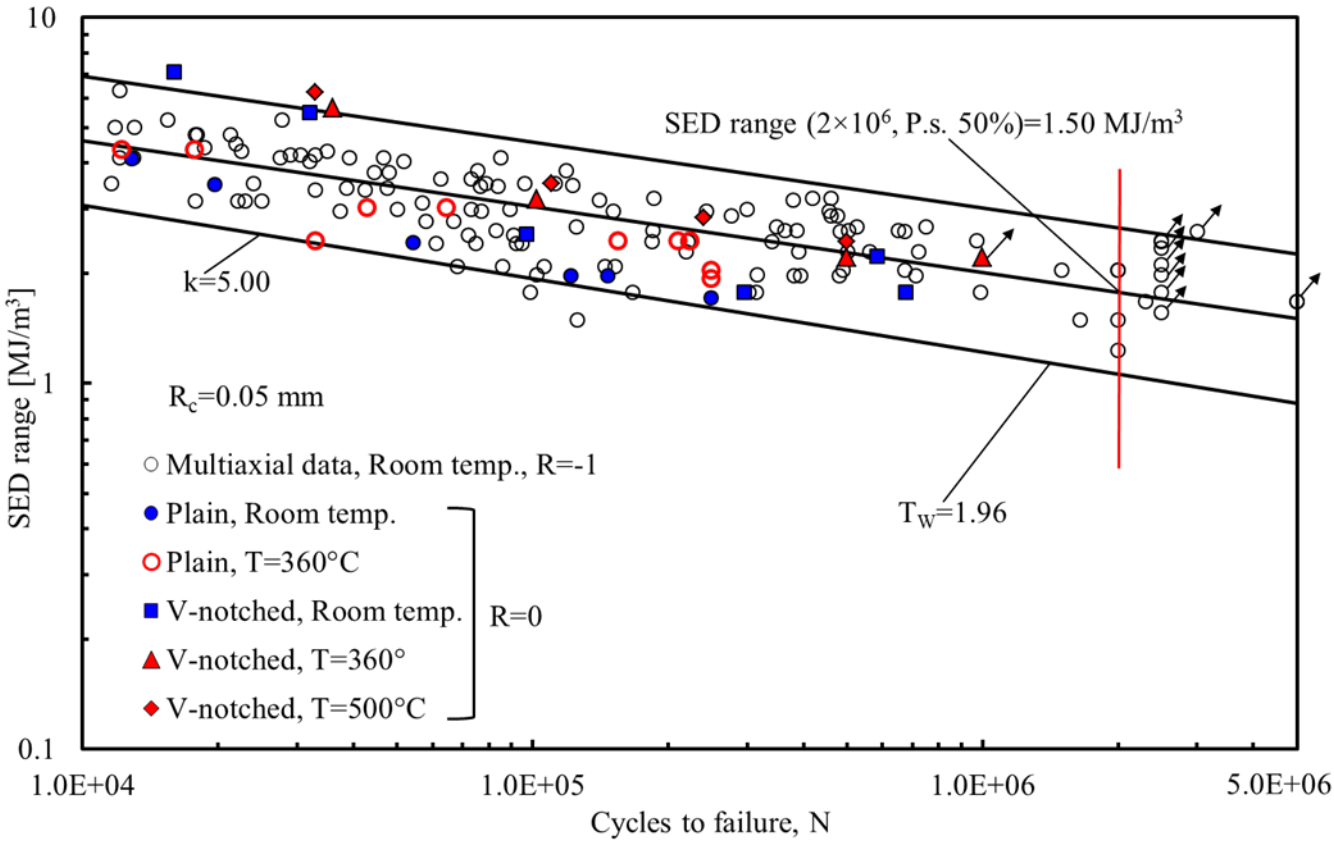

Figure 17. Synthesis by means of local SED of new fatigue data up to 500°C and room temperature multiaxial fatigue data

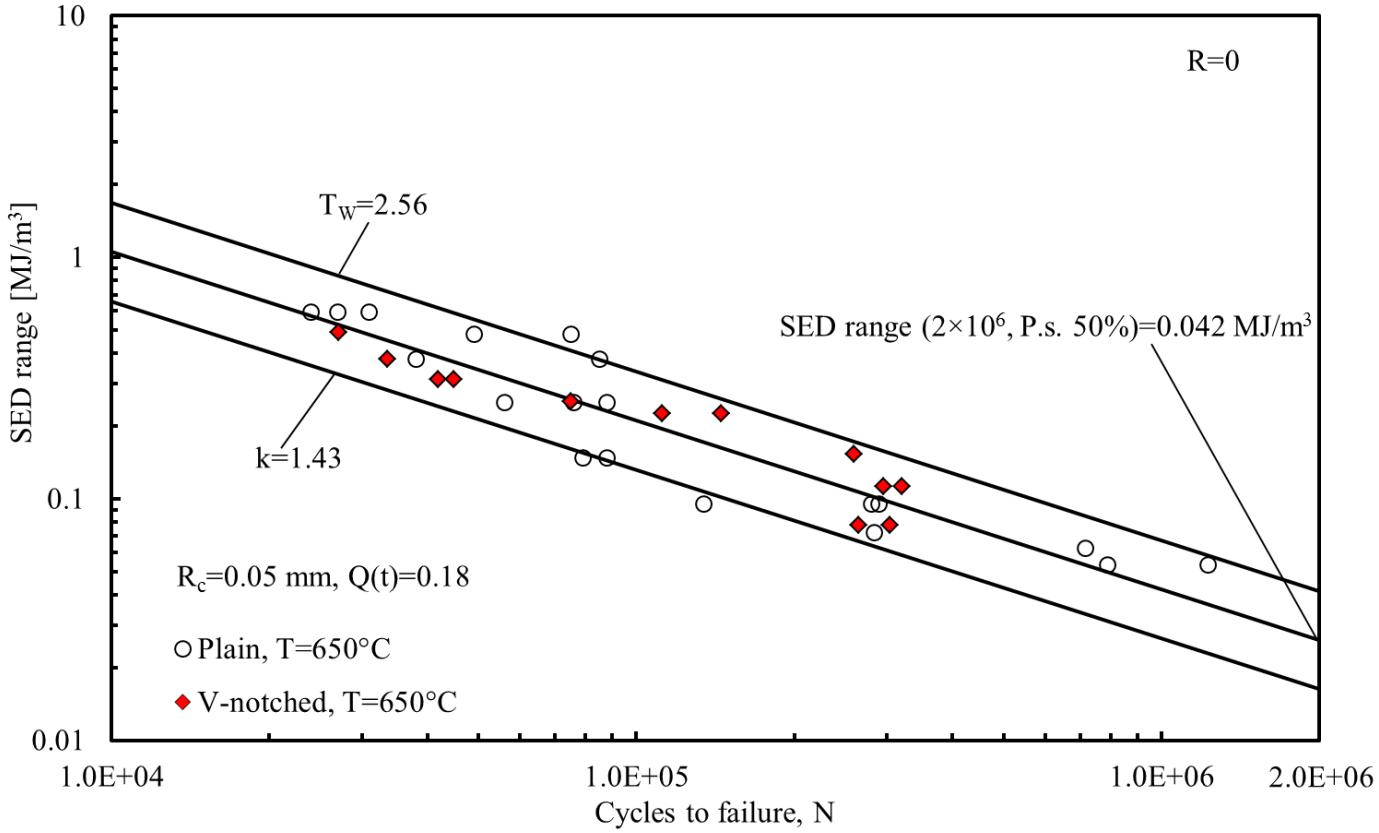

Figure 18. Synthesis by means of local SED of the new fatigue data at 650°C; plain and notched specimens are summarised in the same scatterband.